HAL open science

Solar cell modeling in normal and degraded operations for simulation and monitoring

Mohand Djeziri, Samir Benmoussa, R. Tapia Sanshez, Olivier Palais, Giuseppe Tina

To cite this version:

Mohand Djeziri, Samir Benmoussa, R. Tapia Sanshez, Olivier Palais, Giuseppe Tina. Solar cell modeling in normal and degraded operations for simulation and monitoring. 2023. hal-03533433

HAL Id: hal-03533433

https://amu.hal.science/hal-03533433v1

Preprint submitted on 6 Feb 2023

HAL is a multi-disciplinary open access archive for the deposit and dissemination of scientific research documents, whether they are published or not. The documents may come from teaching and research institutions in France or abroad, or from public or private research centers.

L'archive ouverte pluridisciplinaire **HAL**, est destinée au dépôt et à la diffusion de documents scientifiques de niveau recherche, publiés ou non, émanant des établissements d'enseignement et de recherche français ou étrangers, des laboratoires publics ou privés.

Manuscript File Click here to view linked References

Solar cell modeling in normal and degraded operations for simulation and monitoring

Mohand A. Djeziri[a,*], Samir Benmoussa[b], R. Tapia Sanshez[c], Olivier Palais[d], Giuseppe M. Tina[e]

[a] *Aix-Marseille University, Université de Toulon, CNRS, LIS, Marseille, France*
[b] *Laboratoire d'Automatique et de Signaux de Annaba (LASA), Université Badji Mokhtar, Annaba, Algérie*
[c] *Facultad de Ingenieria Electrica,Division de Estudios de Posgrado Universidad Michoacana de San Nicolas de Hidalgo 58000, Morelia, Mexico*
[d] *Aix-Marseille University, Université de Toulon, CNRS, IM2NP, Marseille, France*
[e] *University of Catania, Catania, Italy*

Abstract

The transition to clean energies is a major environmental and economic issue. The transformation of solar irradiance into electrical energy appears to be one of the most promising solutions thanks to its simplicity of implementation and its worldwide availability. However, the lifespan of solar cells and their efficiency remain open research issues. Improving the performance of solar cells requires in-depth knowledge of this equipment on different levels in normal, degraded and faulty operations. This paper presents a multi-physical modeling of solar cells integrating different phenomena on three levels of abstraction: the material level, the cell level and the panel level. The proposed model highlights the key parameters of the system and their influence on its performance, thus, it is possible to simulate normal operations and degraded operations by introducing variations of the system characteristics. On the material level, the simulation results show that a variation of 1mv in the open circuit voltage causes a variation of 4.68% in the cell power. On the cell level, and after 2000 hours of use of the photovoltaic cell in presence of wear phenomenon, the observed degradation in the cell performance represents a voltage decrease of 38.98% and a 40% current decrease. These results are in agreement with the experimental measurements available in the literature, corroborating the effectiveness of the proposed model.

Keywords: Solar Cell, System-level modeling, material-level modeling, Simulation, monitoring,

1. Introduction

Photovoltaic Renewable Energy (RE) is the most common RE as it is available everywhere. For example, the mean global insulation on horizontal plan is about $1127kWh/m^2$ per year in Paris and $2300kWh/m^2$ per year in the Sahel of Africa [1]. However, the efficiency and the lifespan of photovoltaic panels are to be improved in the aim of promoting the large-scale deployment of this technology. To achieve this improvements, several works are proposed in the literature to model the behaviour of photovoltaic cells in order to identify the key parameters influencing their performances. But the major efforts made by the scientific community for modeling photovoltaic cells on one side, and semiconductor materials on the other side are led separately, and up to our knowledge, there is no generic model of a photovoltaic system integrating several phenomena of degradation, usable for both causal and structural analysis, and allowing the simulation of normal and degraded operations on different abstraction levels.

*Corresponding author
Email addresses: mohand.djeziri@lis-lab.fr (Mohand A. Djeziri), samir.benmoussa@univ-annaba.dz (Samir Benmoussa), roberto.tapia@umich.mx (R. Tapia Sanshez), olivier.palais@univ-amu.fr (Olivier Palais), giuseppe.tina@dieei.unict.it (Giuseppe M. Tina)

On the cell level, two types of models are widely used: the one-diode model and the two-diodes model, associated with a series resistance and a shunt resistance. In some models, the shunt resistance is assumed to be infinite and hence neglected. The two-diodes model is reduced to a one-diode model assuming that the recombination in the space-charge zone can be neglected [2]. A comparative analysis of five of the most used one-diode models is proposed in [3], with a focus on the physical assumptions and techniques used for parameter identification. A two-diodes model of a photovoltaic cell is presented in [4] at different levels of irradiance and temperature. The model parameters are identified by using a derivative method at maximum power point and mountain-climbing algorithm. These equivalent electrical circuits established according to reference values of temperature and incident irradiance are easy to implement and their parameters are simple to identify. However, they don't take into consideration the thermal effect at the cell level (heating caused by resistive effect) which is a determining factor of the cell's performance. Although the cell temperature appears in the models estimating open-circuit voltage and short-circuit current, it is considered as a known or measured parameter. But the transformation of electrical power into thermal power is not modeled. In practice, the cell temperature is not measurable directly because the cells are inside the panels with other layers of material surrounding them. In this manner, when these models are used for efficiency analysis according to the operating temperature and variation in the solar radiation [5], a difference between the laboratory experimental results and the ones observed in real operating conditions is often highlighted [6]. The issue of estimating the cell temperature is addressed in [7], where an overview of the studies dedicated to the analysis of temperature losses in a photovoltaic cell is presented. It demonstrates that the wind, the speed, the positioning of the photovoltaic panel, and the techniques chosen for parametric identification are factors determining the accuracy of existing estimators of temperature losses in a solar cell.

The Bond graph formalism being a multi-physical modeling approach [8], is used to model the matching of the electrical and thermal phenomena in a photovoltaic cell [9]. The causal and structural properties of the bond graph methodology are used in [10] to bring out the algebraic loop between the series and shunt resistances induced by the dual choice of causality of the two resistances, leading to problems of resolution and computing time. This issue is solved by considering a one-diode model, on which a capacitance is added in parallel to the diode. This capacitance represents the depletion region and carrier diffusion, depending on the light and the temperature of the cell. A bond graph model of photovoltaic cells considering thermal effects is presented in [9]. It integrates the capacitor proposed by [10], neglects the series resistance, and allows the simulation of normal operations at the cell level. The issue of model-parameter identification, common to all modeling formalisms, is studied in [11], where both the analytical and the soft computing approaches are analysed.

At the material abstraction level, the fabrication methods of black silicon ($b-Si$) are addressed in [12]. It analyses the application and performance of ($b-Si$) in photovoltaics, and the theoretical modelling efforts in ($b-Si$)-based photovoltaic cells. A review of papers studying the cell cracks presented in [13], submits a classification of cracks, the factors that favour their appearance, as well as the analysis of experimental and numerical studies related to PV cracks. The relationship between interstitial oxygen, substitutional carbon, resistivity and minority carrier lifetime in metallurgical multicrystalline silicon is identified in [14] in order to prevent the Light Induced Degradation (LID) phenomenon and the SiC particles formation. These occurrences are at the origin of the losses in open circuit voltage and shunts in solar cells. The measurement presented in [15] about LID amplitude evolution on cells according to different ingot-height, shows that these degradation have a dependence on the position along the ingot height. In addition, the relationship between the open circuit voltage and the equilibrium electron density is formulated.

Thus, it can be seen that the modeling at the material level of photovoltaic cells is oriented towards empirical models resulting from laboratory experimental tests. The obtained models allows to characterize a set of degradation phenomena, but are not integrated into models of higher level of abstraction (cell and panel levels) to create complete simulators.

In this paper, a dynamic model, based on bond graph formalism, including in the same simulator the material, the cell and the panel aspects in normal and degraded operations is presented. This modeling approach is incremental, highlights cause-and-effect relationships, input-output relationships, and the evolution of the flow of power and information from the material level of abstraction to the panel one. The model is then used to simulate normal and degraded operations at both cell and material levels. At the cell

Abbreviation	Designation	Abbreviation	Designation
RE	Renewable Energy	LID	Light Induced Degradation
PV	Photo Voltaic	RS	Bond Graph RS element
R_x, R_y, R_z	Bond Graph R-element	C	Bond Graph C-element
c	Specific Heat of the material	ρ	The volume mass
n	Thermal conductivity	l_x, l_y, l_z	Longitude of x, y, z axis
v_{cell}	Cell Voltage	i_{ph}	Current supplied by the thermal effect
i_{celle}	Cell Current		and the radiation
i_{RS}	Resistance current	i_d	Diode current
A	Area	G_E	Effective Irradiance
S_r	Spectral averaged responsivity	G_0	Solar Irradiance
K	Temperature coefficient	T	Cell temperature
$R(t)$	Parallel $R_p(t)$ or series $R_s(t)$ resistance	T_0	Ambiant Temperature
R_n	Nominal value of resistance	E_e	Electrical effort
$R_f(t)$	Degradation dynamic	E_f	Electrical flow
v_{oc}	Open circuit voltage	T_e	Thermal effort
n_0	Electron density	T_f	Thermal flow
k_B	Boltzmann constant	q	Electron elementary charge
n_i	Intrinsic carrier concentration	Δp_{front}	Excess minority carrier concentration
IH	Ingot height	c_l	Compensation level

Table 1: Nomenclature

level, the effect of the variation of the ambient temperature, the irradiance, the exposed surface and wear are simulated. At the material level, the influence of the material characteristics on the power production, such as the LID phenomenon, ingot height and concentration of charge carriers are simulated and analysed.

This paper is organised as follows: Section 2 is devoted to the methodology, where the system is described and decomposed into sub-systems, and then models of normal and degraded operations are detailed. Simulation scenarios are defined in Section 3, where the obtained results are analysed and compared to experimental results. Finally, a conclusion and future work are given in Section 4.

2. Methodology

2.1. System description and decomposition

The sun is commonly considered in the literature as a black body that emits light in the visible region of wavelengths, with a power of $1360W/m^2$, reduced by crossing the earth's atmosphere to around $1000W/m^2$ [16]. To capture and transform the energy of solar irradiance into electrical energy, solar cells built from semiconductor materials are used. The widely used semiconductor materials are silicon (Si) and gallium arsenide ($GaAs$). To obtain the semiconductor property, the material is first freed of its impurities, and then secondly doped by adding atoms of phosphorus and boron. At the end of this doping process, N-type silicon with excess electrons (phosphorus doped) and P-type silicon with holes (boron doped) are obtained. The junction of the two types of Silicon (P and N) forms a semiconductor. When the semiconductor is exposed to light, photons eject electrons from their atomic orbitals, they accumulate in the junction to create electric current. The movement of electrons creates a thermal effect (heating) in the cell by a conduction phenomenon which is added to the heating provided by the irradiance. So, at the system level, the interactions of the various physical phenomena can be represented by the diagram of Figure 1. The dynamics of these physical phenomena occurring at the system level depends on the characteristics of the semiconductor material, such as carrier concentration and ingot height.

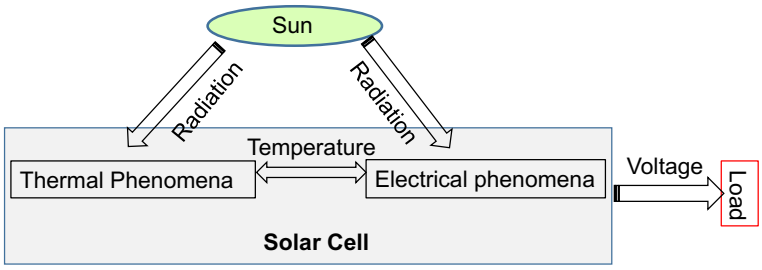

Figure 1: Interaction of physical phenomena in a solar cell

2.2. Modeling of normal operation

Sun irradiance has been the subject of several modeling researches as it is a relevant element in forecasting climatic changes and developing renewable energies [17]. The complexity of the irradiance phanomenon explains the diversity of modeling hypotheses and models proposed in the literature. A comparative analysis of more than seventy models is proposed in [18], where solar geometry inputs and atmospheric parameters inputs required for model implementation are presented, then, the models are given from the simplest to the most complex, specifying that the choice of the irradiance model depends on the model accuracy and the context of use. In this paper, the proposed simulator focuses on the dynamics of the photovoltaic system where the irradiance is considered as an input. Real values of irradiance, measured experimentally and presented in [19], are used as inputs for the validation of the proposed model.

2.2.1. Thermal model

The thermal phenomenon is produced in a photovoltaic cell by the effect of the sun irrradiance, as well as by the electrical phenomenon in the cell which generates heating. A solar cell is made up of several layers, and the heating distribution is assumed homogeneous over the whole cell. To allow the connecting of different layers of the cell in the same model while distinguishing each layer, as well as the resistive and capacitive effects, the bond graph model of a layer is proposed in Figure 2.

In this model, the resistive and capacitive effects appear explicitly, and the exchanges with the other layers and with the environment are highlighted.

The thermal model is composed by two R-elements for each axis (Rx, Ry, Rz) modulated by the following equations:

$$\begin{cases} Rx = \frac{l_x}{\eta l_y l_z} \\ Ry = \frac{l_y}{\eta l_y l_z} \\ Rz = \frac{l_z}{\eta l_y l_z} \end{cases} \tag{1}$$

The C-element represents the structure volume expressed as follows:

$$C = \rho c l_x l_y l_z \tag{2}$$

with c is the specific heat of the material, ρ is the volume mass, and $(l_x, l_y l_z)$ are the longitude of each axis.

2.2.2. Electro-thermal model

The bond graph model of electro-thermal part of the solar cell considered in this work is given in Figure 3, where the electrical part is made up of a diode, a parallel resistor and a series resistor. The thermal effects caused by the presence of resistive elements are taken into account in this model thanks to the use of the bond graph RS-element.

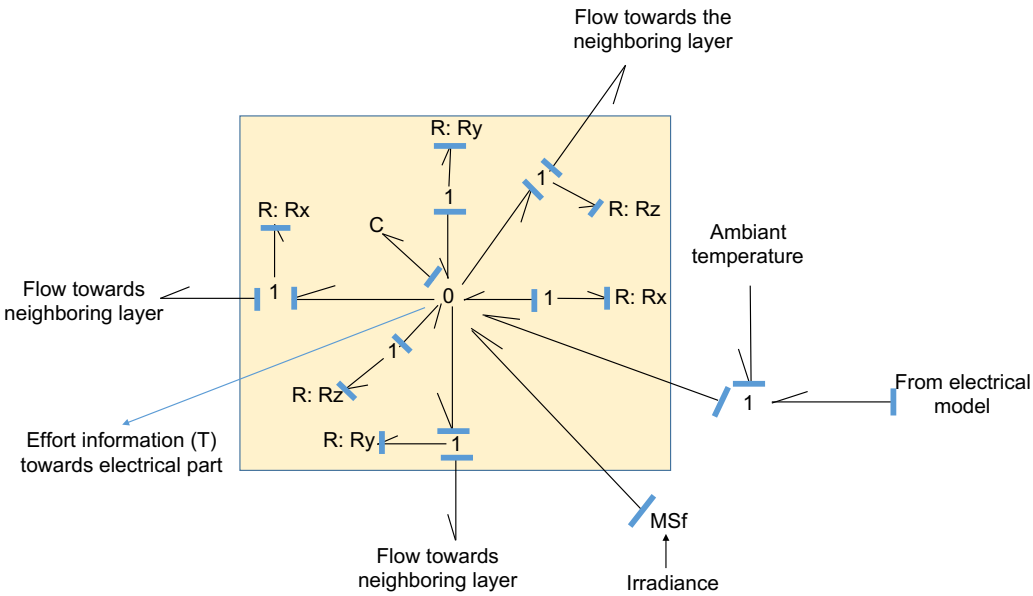

Figure 2: Bond graph model of the thermal phenomena in the solar cell considering a single layer and highlighting the matching with the other layers, the environment and the electrical model.

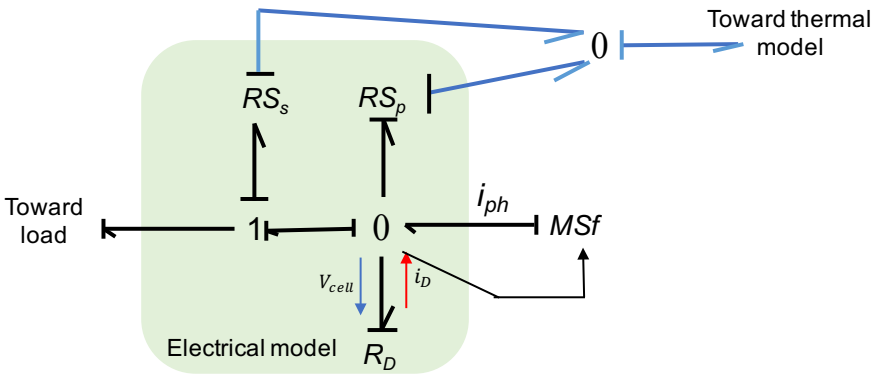

Figure 3: Bond graph model of the electro-thermal part of the solar cell

The diode R_D and the resistance RS_p are associated with the bond graph element of junction 0, which means that they are in parallel. These two elements are associated with the resistance RS_s by a junction 1, which means that all of the elements (RS_p and R_D) are in series with the resistance RS_s.

At the junction 0 of the bond graph model of Figure 3, the effort (v_{cell}) is conserved and the cell current i_{cell} is given by the following equation:

$$i_{cell} = i_{ph} - i_D - i_{RS} \tag{3}$$

i_{ph} is the current supplied by the thermal effect and the radiation, and approximated by the following equation:

$$i_{ph} = A.G_E.S_r.K\left(T - T_0\right)\frac{G_E}{G_0} \tag{4}$$

where K is is the temperature coefficient ($K = 0.0017A/K$ for a silicon solar cell). A is the area, G_E is the effective irradiance, G_0 the solar irradiance, S_r is the spectral-averaged responsivity, T is the cell temperature and T_0 the ambient temperature. The diode is represented by the non-linear R-element, noted R_D and modulated by the following expression:

$$\begin{cases} i_D = i_{cc} C_1 exp\left(\frac{v_{cell} - \Delta v_{cell}}{C_2 v_{oc}}\right) \\ \Delta v_{cell} = v_{oc} \Delta v_{oc} \left(T - 298\right) \end{cases} \tag{5}$$

where i_{cc} is the shut-current, v_{oc} is the open circuit voltage and i_D the diode current. C_1 and C_2 are constants.

To better understand the coupling of electrical and thermal effects, let us recall the operating principle of a RS element [20]. The bond graph model of the RS element is given in Figure 4. The symbol R indicates a resistive element associating an algebraic relationship between effort and flux (like an electrical resistance: $u - Ri = 0$ where u is the voltage and i the current). To include the thermal effects in the case where this resistance heats up and gives off heat, the the symbol S (as source) is added. The RS element then takes heat generation into account.

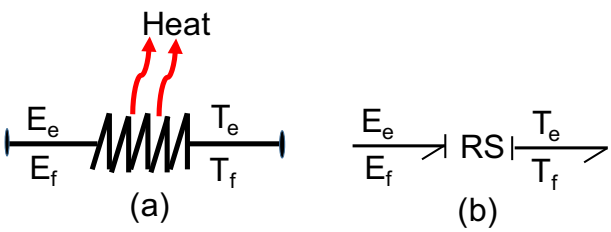

Figure 4: RS element: (a) Heating resistance. (b) its bond graph model

In the case of a simple causality where only one of the two power variables is known (the effort or the flow) at the input of the RS-element, the power delivered is a nonlinear function of the known power variable and the value of the parameter RS. The RS-element is modulated by the following system of equations:

$$\begin{cases} E_e = (R(t) * T_e) + E_f \\ T_f = \left(\frac{(E_e)^2}{R(t)}\right) T_e \end{cases} \tag{6}$$

E_e and E_f are respectively the electrical effort and electrical flow. T_e and T_f are respectively the thermal effort and thermal flow. $R(t)$ is the parallel or series resistance.

2.3. Full Model of normal operation

The full model of a solar panel made up of 8 cells stacked four by four is given in Figure 5. The model highlights the modular and multi-physical aspect of the model, where the inputs and outputs of each subsystem (module) appear explicitly, allowing thus the arrangement of the modules in a library of reusable and individually perfectible models, while keeping clearly visible the cause and effect relationships with the other modules. The bond graph model allows a geometric representation of the stacking of cells, by differentiating the cells exposed to the sun from those which are not exposed, and highlights the power matching between the cells. So, it is possible to build panels of different surfaces only by adding cell modules. The parameters of the full model keep a clear physical meaning, as they correspond to well identified physical phenomena and components. This property is used to simulate normal operating of the cell, and degraded situations by replacing the nominal bond graph element (constant identified in normal operation) by the degradation model of the considered bond graph element.

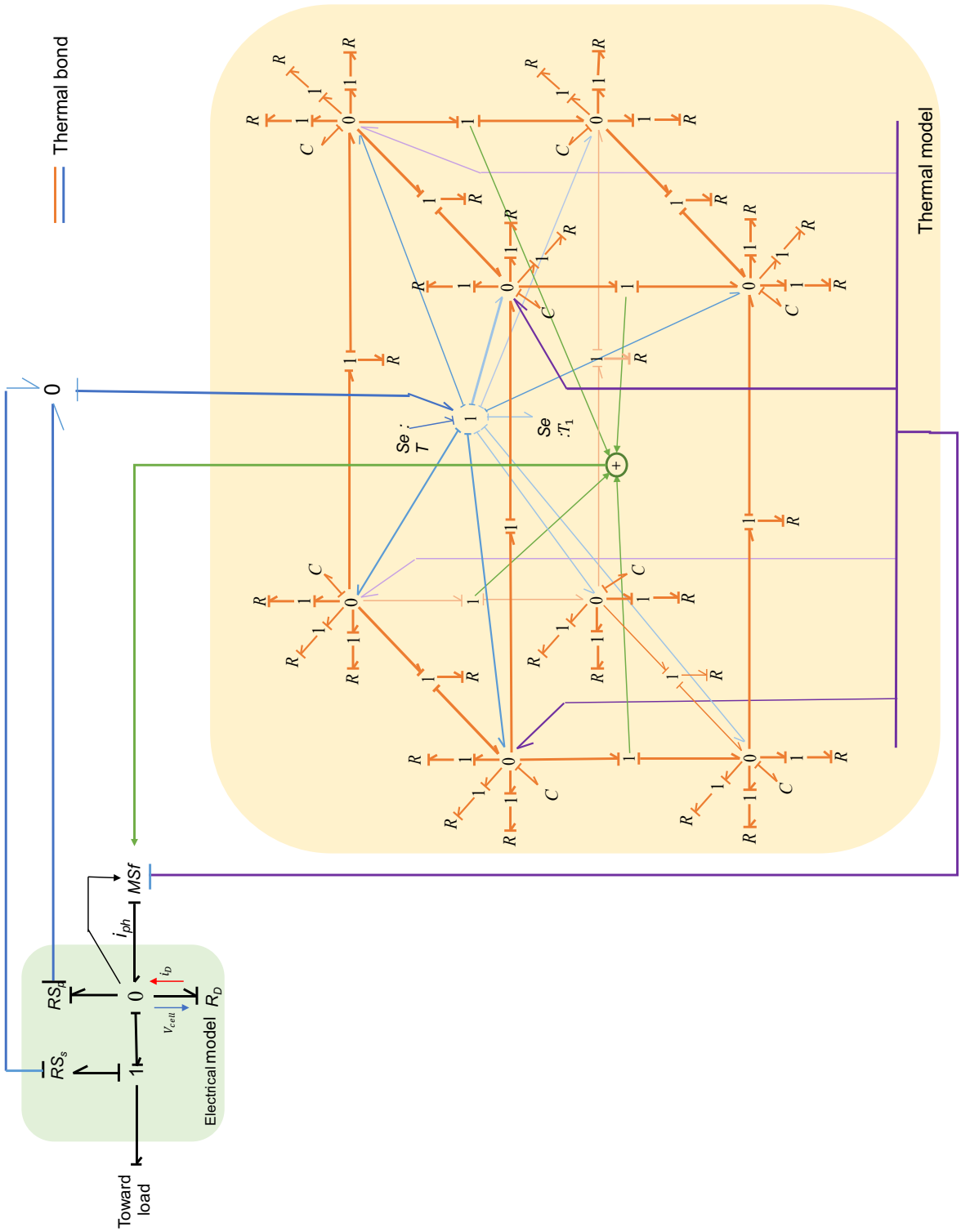

Figure 5: full model of a solar panel made up of 8 cells

Time $[Year]$	$R_{pf}(t)[Ohm]$	$R_{sf}(t)[Ohm]$
0	185	0.53
5	173	-
10	163	0.548
15	155	-
20	146	0.539
25	138	-
30	130	0.568
40	-	0.579

Table 2: variation of the parallel resistance $R_{pf}(t)$ and series resistance $R_{pf}(t)$ under accelerated ageing conditions [22]

2.4. Modeling of the degradation phenomena

In the presence of degradation, and according to the degradation type, the bond graph elements affected by the degradation are the diode R_D and the two resistor RS_p and RS_s. The following section presents the formal relations which relate the dynamics of degradation to the dynamics of the bond graph elements RS_p, RS_s and R_D.

2.4.1. Wear

It has been demonstrated experimentally in [21] that the wear phenomenon of the photovoltaic cell linked to ageing, results in a variation of the parallel and series resistances. In the model of normal operation, these two resistances are the variable $R(t)$ which appears in the nonlinear formula of the element RS given by Eq.6. To differentiate the series resistance from the parallel resistance, the series resistance is noted $R_s(t)$ and parallel one is noted $R_p(t)$.

The conditions of the accelerated ageing test conducted by Hulkoff et al. [21] are: sample consisting of a monocrystalline silicon cell encapsulated with EVA (ethylene-vinyl acetate) and glass, heat $360°K$, relative humidity 85%. The measurements are taken every $500h$ (equivalent to 10 years of use under normal conditions). The results obtained, given in Table. 2, are used to fit the variation models of the resistances. For the two resistances ($R_s(t)$ and $R_p(t)$) the degradation dynamic is additive to the nominal value of the resistance as given by Eq.(7).

$$R(t) = R_n + R_f(t) \tag{7}$$

R_n is the nominal value of the resistance $R(t)$ and $R_f(t)$ is the degradation dynamic given in Eq.8 for the parallel resistance $R_{pf}(t)$ and Eq.(9) for the series resistance.

$$R_{pf}(t) = 0.01826t^2 - 2.35239t \tag{8}$$

$$R_{sf}(t) = 0.00122t \tag{9}$$

Th numerical values of the parameters are identified using the experimental measurement given in Table. 2[22].

2.4.2. Ethylene Vinyl Acetate discoloration

In [23], F.J Pern explained the ultraviolet light degradation, and showed how the Ethylene Vinyl Acetate (EVA) discoloration occurs over time. This phenomenon causes a series resistor increase and a parallel resistance decrease. For the two resistances ($R_s(t)$ and $R_p(t)$), as for the wear phenomenon, the degradation dynamic is additive to the nominal value of the resistance as given above (Eq. 7).

The degradation caused by the EVA discoloration is given by Eq.(10) for the series resistance $R_{sf}(t)$ and Eq.(11) for the parallel resistance $R_{pf}(t)$.

$$R_{sf}(t) = 9.9 \cdot DYI \cdot 10^{-3} \tag{10}$$

IH [%]	C_l	v_{oc} [mV]	n_0
2	11.4	585	10.7
30	7.4	606	12.8
43	-	606	12.9
58	4.3	619	14
86	3.2	622	13.7

Table 3: evolution of C_l, v_{oc} and n_0 according to the variation of the IH.

$$R_{pf}(t) = -193 \cdot DYI \tag{11}$$

With DYI is the Delta Yellowness Index.

2.4.3. Light-Induced Degradation

The Conversion efficiency is proportional to the open circuit voltage v_{oc} as demonstrated in [24, 25]. Under illumination, the electrical performance of solar cells gradually decreases. This is called Light-Induced Degradation (LID). LID is due to the presence under illumination of recombination-active complexes associating an interstitial O dimer ($Oi2$), and a B atom (substitutional (Bs)) or interstitial (Bi) reducing the carrier lifetime. Results based on compensated Czochralski (Cz) $p-Si$ show that the concentration of BO_{i2} complexes depend on the net doping, characterised by the equilibrium electron density, i.e. $[B]$–$[P]$ [15]. This behaviour could be explained by an association of a B atom with a P atom, forming BP pairs.

The variation of the open circuit voltage v_{oc} according to the the equilibrium electron density n_0 is given as follows [15]:

$$v_{oc} = \frac{k_B T}{q} ln\left(\frac{\Delta p_{front} n_0}{n_i^2}\right) \tag{12}$$

n_0 is the equilibrium electron density, equal to $[B]$–$[P]$, $k_B T$ is the Boltzmann thermal energy, q is the electron elementary charge, Δp_{front} is the excess minority carrier concentration and n_i is the intrinsic carrier concentration.

The equilibrium electron density depends on the concentration of charge carriers (compensation level), and its variation can be expressed as follows [15]:

$$n_0 = \frac{[B] + [P]}{C_l} \tag{13}$$

where C_l is the compensation level.

The compensation level is related to the height of the ingot (IH) as well as the manufacturing process of the semiconductor material. This relationship is complex because the knowledge about the physical phenomena is not sufficiently established to take hypotheses and build a physical model. This relation has been demonstrated by experimental results. A set of experimental data highlighting the relationship between IH, C_l, v_{oc} and n_0 is given in Table. 3. Each result in this table is an average of three cells results.

The data-set of Table. 3 is used in this paper to build three data-driven models that can be used in different configurations according the known variable:

- The first model describes the evolution of C_l as a function of IH. In this case the model input is IH:

$$C_l = 0.001(IH)^2 + 0.186(IH) + 11.87 \tag{14}$$

- The second model describes the evolution of v_{oc} as a function of C_l. In this case the model input is C_l:

$$v_{oc} = -0.118(C_l)^3 + 2.53(C_l)^2 20.71(C_l)^3 + 667.1 \tag{15}$$

- The third model describes the evolution of v_{oc} as a function of IH. In this case the model input is IH:

Input	Output	Model	Accuracy
I_H	v_{oc}	$v_{oc} = 15.12(I_H)^{0.2814} + 566.6$	SSE = 48.73 R^2 = 0.9535
I_H	C_l	$C_l = 0.001(I_H)^2 + 0.186(I_H) + 11.87$	SSE = 0.1682 R^2 = 0.9968
Cp	v_{oc}	$v_{oc} = -0.118(C_l)^3 + 2.53(C_l)^2 20.71(C_l)^3 + 667.1$	SSE = 28.41 R^2 = 0.9729

Table 4: Summary of the fitted models and their accuracy

$$v_{oc} = 15.12(IH)^{0.2814} + 566.6 \tag{16}$$

A summary of the obtained models and their accuracy is given in Table. 4. The fitting results of the three models are shown in Figure 6.

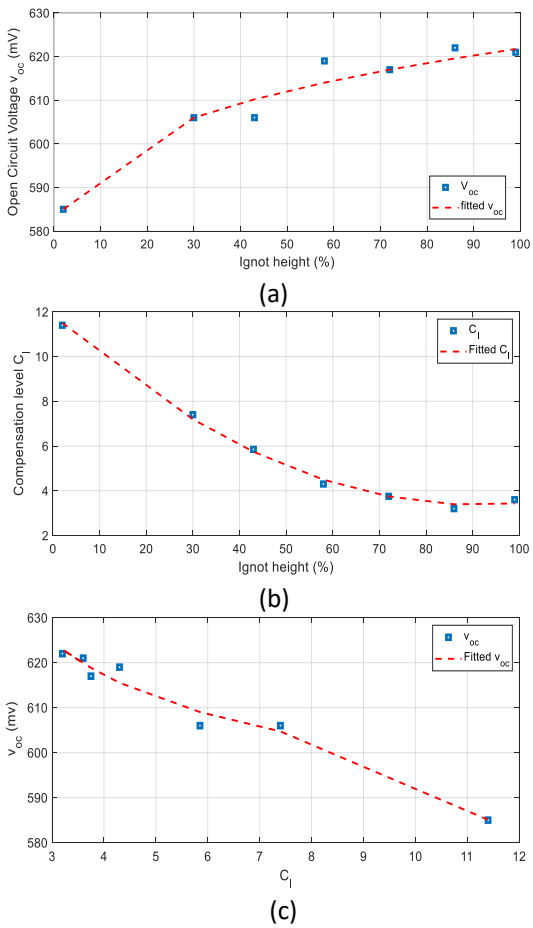

Figure 6: Fitting Results: (a): $v_{oc} = f(IH), (b) : C_{ol} = f(IH), (c) : v_{oc} = f(C_l)$

These three configurations will make it possible to simulate the effect of IH on C_l and consequently on

v_{oc}, the effect of IH on v_{oc} independently of C_l, and the effect of C_l on v_{oc} independently of IH.

As formalised in Eq.(5) and illustrated in Figure 3, the element R_D is a nonlinear function whose input is the variable v_{cell} and the output is the variable i_D which is a function of v_{oc} (Eq.5). The experimental characterisation of the LID phenomenon shows that this phenomenon causes a variation of v_{oc} through the variation of C_l or of IH (Eqs.(12 to 16)). So, the phenomenon of LID can be introduced in the bond graph model by estimating v_{oc} from Eq.(12 to 16).

3. Results and discussion

3.1. Simulation of the normal operation

The first simulation scenario represents the variation in the characteristics of a solar cell, according to changes in irradiance conditions and ambient temperature over a period of 24 hours. The ambient temperature and the irradiance used as input of the simulators are real data (ref) recorded over 24 hours and given in Figure 7 [19].

Figure 7 shows a consistent variation in ambient temperature and irradiance which begins to increase when the sun appears at the horizon, then reaches their maximum values at midday with $868.9W/m^2$ around $1p.m.$ for irradiance and $306.5K°$ around $3p.m.$ for ambient temperature. The two variables begin to decrease in the second part of the day to reach $300°K$ for temperature and $0W/m^2$ for irradiance.

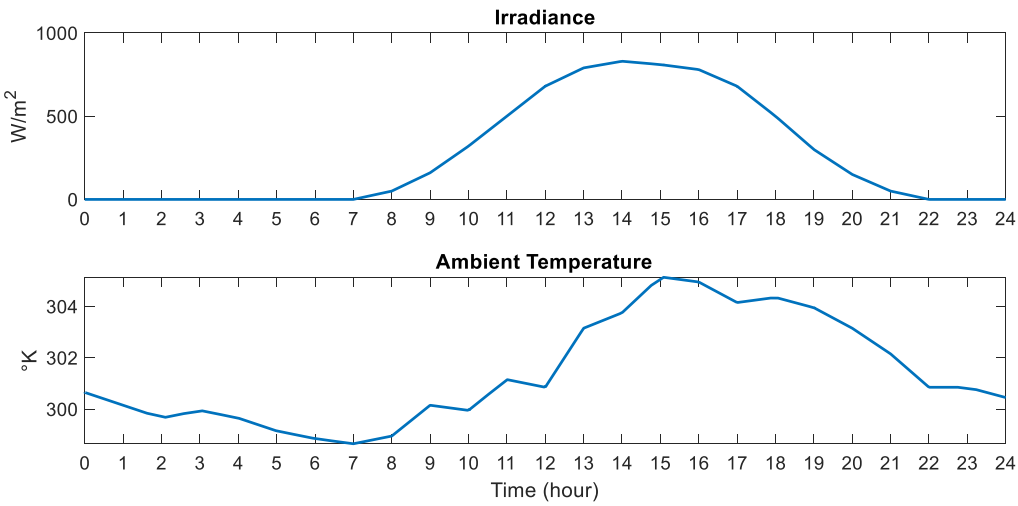

Figure 7: data acquired by the meteorological station for a typical clear sky day on 15 July 2011 presented in [19].

To assess the effect of individual variation in irradiance, temperature and cell area exposed to the sun on the performance of the solar cell, three scenarios are considered:

- In the first scenario the irradiance varies in stages ($500W/m^2, 750W/m^2$ and $1000W/m^2$). The ambient temperature and exposed surface are considered constant: $290°K$ for the ambient temperature and $0.01m^2$ for the surface.

The result obtained is presented in Figure 9, which shows that the electrical power produced by the photovoltaic cell is proportional to the irradiance. This consistent result shows the relevance of the proposed model, but the irradiance being a non-controllable input to the system, this information cannot be used to increase the performance of the photovoltaic cell.

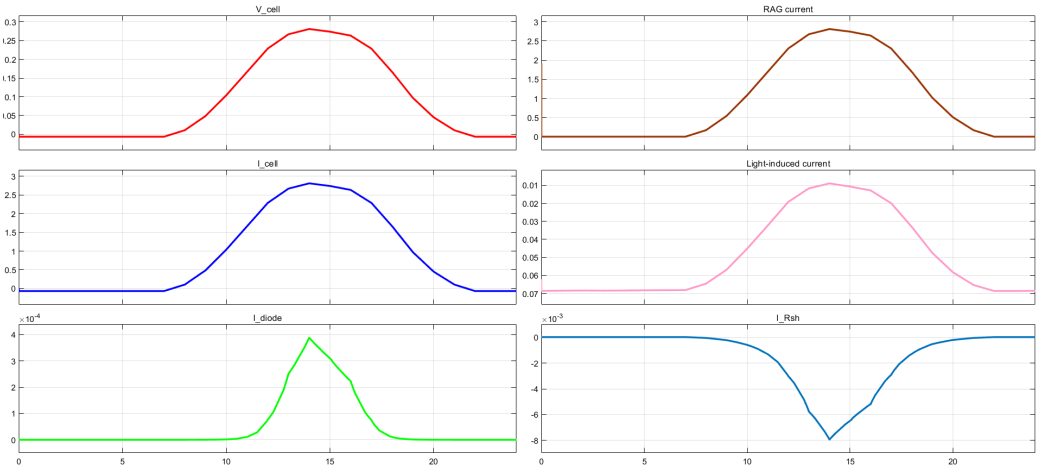

Figure 8: Evolution of the cell voltage v_{cell} and the cell current i_{cell}, the diode current i_D, the current passing through the resistance i_R of the electrical part of the system, the $RAG_{current}$ and the light-induced current according to the variation of ambient temperature and irradiance.

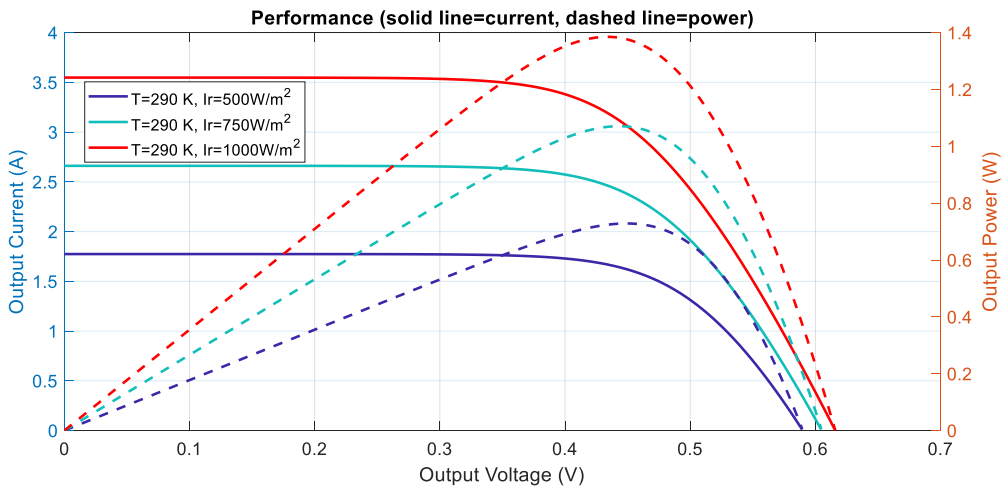

Figure 9: Evolution of the cell performance according to the variation of effective irradiance ($500W/m^2, 750W/m^2$ and $1000W/m^2$). The ambient temperature and exposed surface are considered constant: $290°K$ for the ambient temperature and $0.01m2$ for the surface.

- In the second scenario, the ambient temperature varies in steps of $20°K$ $(280°K, 300°K and 320°K)$, the irradiance and the exposed surface are considered constant: $1000W/m^2$ for the irradiance and $0.01m^2$ for the area.

The result presented in Figure 10 shows that the electrical power produced by the photovoltaic cell is inversely proportional to the ambient temperature which is also an input imposed by the environment. Like irradiance, the ambient temperature cannot be regulated in the absolute case, but the heating that it induces on the cell surface can be limited or regulated by using isolation devices without reducing the irradiance received by the cell and by insuring a rapid evacuation of the heat generated by the cell. Submerged solar

panel is one of the solutions proposed in the literature for cooling the system without reducing significantly the irradiance [26, 27].

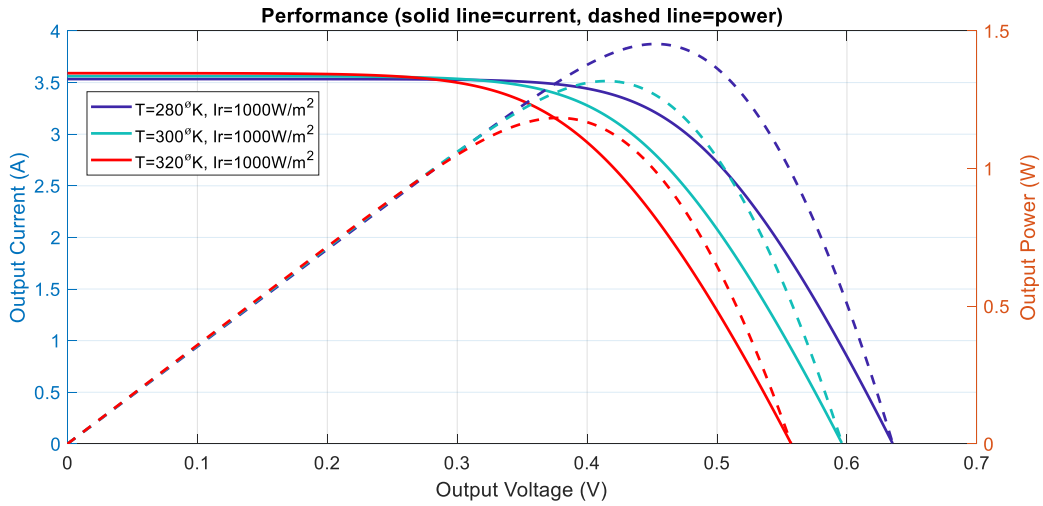

Figure 10: Evolution of the cell performance according to the variation of ambient temperature ($280°K, 300°K$ and $320°K$). The irradiance and the exposed surface are considered constant: $1000W/m^2$ for the irradiance and $0.01m^2$ for the area.

Thus, the presence of the sun increases the irradiance which is proportional to the electrical power produced by the cell, but the presence of the sun heats the system, and heating reduces the performance of the cell. One of the solutions proposed in the literature is cooling the cell with water. The heated water is then returned to the user for home use. This solution, although effective, consumes power. The model proposed in this paper can be used to assess the relevance of these devices by estimating the power gain provided by the temperature control devices and the power required for their operation [26] [28].

In the third scenario, a variation in stages of the exposed surface is simulated ($0.005m^2, 0.01m^2, 0.02m^2$). The irradiance and the ambient temperature are considered constant: $1000W/m^2$ for the irradiance and $290°K$ for ambient temperature.

The result of simulating the variation of the cell-surface exposed to the sun is shown in Figure 11. This figure highlights the great influence of this parameter on the electrical power produced by the photovoltaic cell. In fact, by doubling the exposed surface we almost double the power produced. In addition, the exposed surface is a parameter that can be regulated by the installation of a set of sensors and actuators for the detection of the sun position and the automatic orientation of the cell using motors [29]. But again, this technological solution consumes power, so the ratio between the gain in power provided by the optimisation of the exposed surface and the power required for the automatic orientation of the cell must be studied [30, 31].

3.2. Simulation of the degraded operations

3.2.1. Simulation of the cell performance according to the LID phenomenon

The evolution of v_{cell}, i_{cell}, and P_{cell} according to the experimentally measured variations of v_{oc}, are given in the Figure 12. This result obtained for $24hours$ of operation under the temperature and irradiance conditions given in Figure 7, shows that the variation in the characteristics of the PV cell is relatively small. To be able to illustrate it, only a window of $15minutes$ of variation is shown in Figure 12.

To better highlight the dynamic of cell characteristics (v_{cell}, i_{cell} and P_{cell}) according to the materials ones (IH, C_l and v_{oc}), a simulation is carried out from the experimental data presented in [15]. Then, The average and maximum values of v_{cell} i_{cell}, P_{cell} and v_{oc} are calculated and given in Table. 5. These results are obtained for $24hours$ of operation under the temperature and irradiance conditions given in Figure 7.

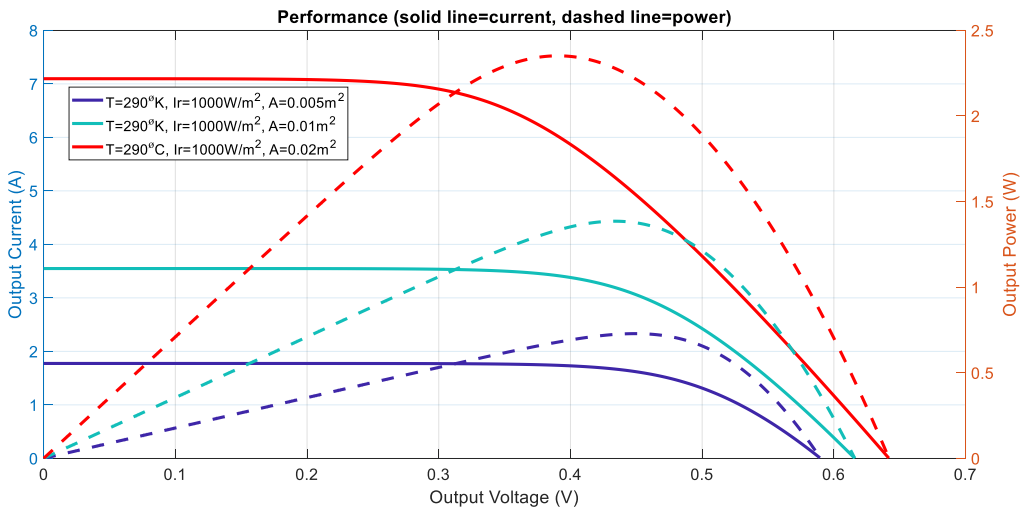

Figure 11: Evolution of the cell performance according to the variation of the surface area of $(0.005m^2, 0.01m^2, 0.02m^2)$. The irradiance and the ambient temperature are considered constant: $1000W/m^2$ for the irradiance and $290°K$ for ambient temperature.

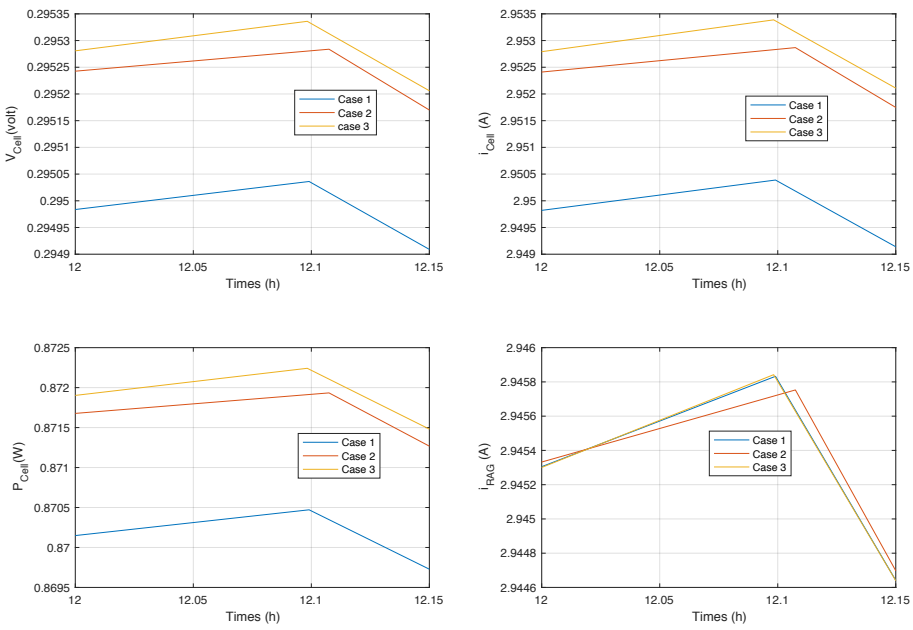

Figure 12: Evolution of the cell voltage $v_{cell}$and the cell current i_{cell}, the cell power P_{cell} according to the variation of v_{oc} in three cases: case 1: $v_{oc} = 500mv$, case 2: $v_{oc} = 600mv$, case 3: $v_{oc} = 700mv$

The relative variations of v_{cell} i_{cell}, P_{cell} are calculated as a percentage for one millivolt of variation in v_{oc}. The results are given in the Table.6, and show that $1mv$ of v_{oc} variation causes a variation of the

IH	C_l	v_{oc}	$v_{cell}Max$	$v_{cell}Mean$	$i_{cell}Max$	$i_{cell}Mean$	$P_{cell}Max$	$P_{cell}Mean$
2	11.4	0.585	2.2953	0.0793	0.9527	0.7933	0.8718	0.1786
30	7.4	0.606	0.2953	0.0797	2.9527	0.7970	0.8719	0.1795
58	4.3	0.619	0.2953	0.07942	2.9529	0.7937	0.8720	0.1788
86	3.2	0.622	0.2953	0.0794	2.9529	0.7939	0.8720	0.1788
-	-	0.700	0.2953	0.0833	0.9534	0.8328	0.8722	0.1871

Table 5: Variations of cell characteristics (v_{cell}, i_{cell} and P_{cell}) according to the materials ones (IH C_l and v_{oc}) for 24$hours$ of operation under the temperature and irradiance conditions given in Figure 7.

$v_{cell}Mean$	$i_{cell}Max$	$i_{cell}Mean$	$P_{cell}Max$	$P_{cell}Mean$
4.86%	0.0.23%	4.74%	0.045%	4.54%

Table 6: The relative variations of v_{cell} i_{cell}, P_{cell} are calculated as a percentage for one millivolt of variation in v_{oc} for 24$hours$ of operation under the temperature and irradiance conditions given in Figure 7

average value of v_{cell} over 24$hours$ of operation of approximately 4.68%, of the average value of i_{cell} of approximately 4.74% and the average P_{cell} value of about 4.54%. The result of Table.6 shows that it is possible to increase the performance of a solar cell by improving the quality of the semiconductor material (by reducing impurities and increasing the concentration of charge carriers, etc.), but the Table.6 also shows that the gain in performance is relatively small compared to the substantial cost that the development of solar panels based on purer semiconductor materials would represent, especially since the cost of implementation being one determining factors in the large-scale development of renewable energy production technology.

3.2.2. Simulation of the cell performance according to the wear phenomenon

Figure 13 shows the evolution of the voltage and current of a photovoltaic cell in the presence of the phenomenon of wear over 2000$hours$ of operation under the condition of temperature and irradiance given in Figure 7, moist of 85% and heat of $360°K$. This figure shows that after 2000 hours of use of the photovoltaic cell under normal operating conditions, the degradation of the performance level is important, it represents a decrease of 38.9831% for v_{cell} and 40% for i_{cell}.

These simulation results can be used in the dimensioning of the systems of production of electrical energy, in order to quantify and then take into account the decreases in performance caused by degradation. To better illustrate, let us consider the Solar / Wind / Diesel / Battery Power System proposed in [32] for off-grid use in remote areas, and optimised for use in the location of Vellore in India. Based on an average solar irradiance of $5.14kWh/m2$ per day, an annual average wind speed of $5.07m/s$, and a diesel price of 1.05 dollars per litter, the device was dimensioned as follows: a $28.3kW$ photovoltaic array, an $8kW$ wind turbine, a $13kW$ diesel generator, 74 battery units and a $12.6kW$ converter.

This RE solution gives a net present cost (NPC) of $166,400$ dollars versus a CNP of $977,523$ dollars for the stand-alone diesel system, which is 488% higher than the proposed design [32]. The proportion of energy production for each part of the system is as follows: solar energy generates approximately 75.8%, while 20.5% is generated by wind turbines and 3.68% is generated from diesel out of the overall annual output.

By taking into account the decrease in performance highlighted in this paper, which is about 39% over 2000 hours of use (which corresponds to around 7 years of operation). The share of power generated by the PV will decrease from 75.8% to 46.2380% of the production of the whole system after 7 years of use, i.e. a difference of 29.5620%. Thus, after 7 years of use, the part of the diesel power will increase from 3.68% to 33.24%.

It is stated in [32] that the ER system consumes 629 Litters of diesel per year at a cost of 1.05 per litter, which gives 660.45 dollars per year. By considering the decrease in PV performance After 7 years of operating, the system will consume 5681.5 litters of diesel with a cost of 5965.6 dollars per year, i.e. an additional cost of 5305.2 dollars per year. These results show that the large-scale use of PV systems will result in a significant improvement in their lifespan.

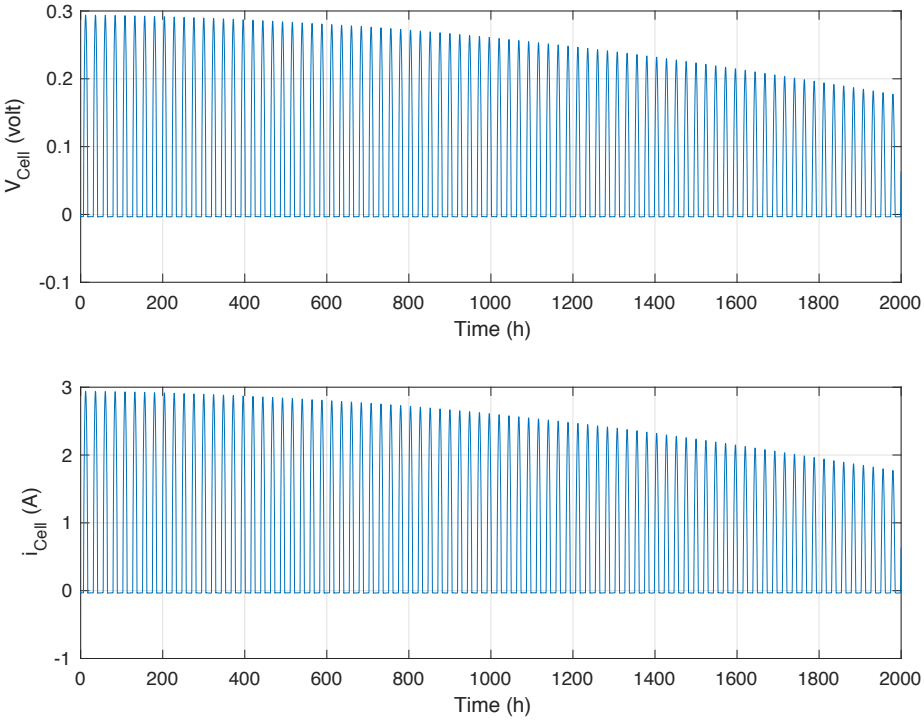

Figure 13: Evolution of v_{cell} and i_{cell}over a period of 2000 hours of use in presence of wear degradation.

4. Conclusion and future work

In this paper, a multi-physical model for simulating normal and degraded operations, at the system level and at the material level is proposed. The model is presented in a modular form where the power interactions between the subsystems are well defined, which allows the stacking of cells by differentiating the exposed cells to the sun from the non-exposed ones. The physical sense of the parameters appears explicitly on the model, allowing the simulation of different degradation phenomena at different levels of abstraction. At the cell level, the effects of a variation in ambient temperature, solar irradiance, exposed surface and wear phenomenon are simulated, showing that after 2000 hours of use in presence of wear phenomenon, the cell performance presents 38.98% of decrease in the cell voltage and 40% in the cell current. At the material level, the influence of the ingot height and the concentration of charge carriers are simulated, and their influence is evaluated, showing that a variation of 1mv in the open circuit voltage causes a variation of 4.68% in the cell power. These results show that the wear is a degradation phenomenon which causes a significant loss of performance, even under normal conditions of use. It is necessary to emphasis that like all modeling approaches, the accuracy of the bond graph model strongly depends on the techniques used for parameter identification.

This model will contribute to the in-depth understanding of the system dynamic and consequently to increase performance of solar cells. It will be used in our future work to generate data-sets for degraded and faulty operations, in presence of multiple and progressive faults, in order to supplement existing experimental databases. These data-sets will be used for learning data-driven algorithms of fault diagnosis, failure prognosis and fault tolerant control, and then the implementation of predictive and conditional maintenance strategies.

References

[1] M. R. Starr, W. Palz, Photovoltaic power for europe. an assessment study, Reidel Publishing Company ISBN: 90-277-1556-4 (1983) 212.

[2] A. N. Celik, N. Acikgoz, Modelling and experimental verification of the operating current of mono-crystalline photovoltaic modules using four- and five-parameter models, Applied Energy 84 (2007) 1–15.

[3] G. Ciulla, V. L. Brano, V. D. Dio, G. Cipriani, A comparison of different one-diode models for the representation of i–v characteristic of a pv cell, Renewable and Sustainable Energy Reviews 32 (2014) 684–696.

[4] Z. Meng, Y. Zhao, S. Tang, Y. Sun, An efficient datasheet-based parameters extraction method for two- diode photovoltaic cell and cells mode, Renewable Energy 153 (2020) 1174–1182.

[5] A. B. Kebede, G. B. Worku, Comprehensive review and performance evaluation of maximum power point tracking algorithms for photovoltaic system, Global Energy Interconnection 3 (2020) 398–412.

[6] C. Schuster, Analytical framework for the assessment and modelling of multi-junction solar cells in the outdoors, Renewable Energy 152 (2020) 1367–1379.

[7] I. Santiago, D. Trillo-Montero, I. Moreno-Garcia, V. Pallarés-Lopez, J. Luna-Rodríguez, Modeling of photovoltaic cell temperature losses: A review and a practice case in south spain, Renewable and Sustainable Energy Reviews 90 (2018) 70–89.

[8] D. Karnopp, D. Margolis, R. Rosenberg, System dynamics: modeling, simulation, and control of mechatronic systems, 5th ed. Hoboken, NJ: John Wiley and Sons.

[9] R. Tapia-Sanchez, A. Medina-Rios, N. Villa-Villasenor, Solar cell model: a bond graph approach, Simulation: Transactions of the Society for Modeling and Simulation International 91 (2015) 349–359.

[10] V. N. Madansure, S. Banerjee, A. Mukherjee, al, Modelling and simulation of pv-powered intermittent load systems by bond graph technique, Simulation: Transactions of the Society for Modeling and Simulation International 55 (1995) 367–375.

[11] V. J. Chin, Z. Salam, K. Ishaque, Cell modelling and model parameters estimation techniques for photovoltaic simulator application: A review, Applied Energy 154 (2015) 500–519.

[12] J. Chai, B. Wong, S. Juodkazis, Black-silicon-assisted photovoltaic cells for better conversion efficiencies: a review on recent research and development efforts, Materials Today Energy 18 (2020) 100539.

[13] L. Papargyri, M. Theristis, B. Kubicek, T. Krametz, C. Mayr, P. Papanastasiou, G. E. Georghiou, Modelling and experimental investigations of microcracks in crystalline silicon photovoltaics: A review, Renewable Energy 145 (2020) 2387–2408.

[14] V. Yen, O. Palais, M. Pasquinelli, D. Barakel, I. Perichaud, Relationship between interstitial oxygen, substitutional carbon, resistivity and minority carrier lifetime in metallurgical multicrystalline silicon, Applied Energy (2011) DOI: 10.24084/repqj09.469.

[15] T.Schutz-Kuchly, S. Dubois, J. Veirman, Y. Veschetti, D. Heslinga, O. Palais, Light-induced degradation in compensated n-type czochralski silicon solar cells, Phys. Status Solidi 208 (2011) 572–575.

[16] J. A. Ruiz-Arias, C. A. Gueymard, Worldwide inter-comparison of clear-sky solar radiation models: Consensus- based review of direct and global irradiance components simulated at the earth surface, Solar Energy 182 (2018) 10–29.

[17] C. Gueymard, V. Lara-Fanego, M. Sengupta, Y. Xie, Surface albedo and reflectance: Review of definitions, angular and spectral t effects, and intercomparison of major data sources in support of advanced solar irradiance modeling over the americas, Solar Energy 182 (2019) 194–212.

[18] F. Antonanzas-Torres, R. Urraca, J. Polo, O. Perpiñán-Lamigueiro, R. Escobara, Clear sky solar irradiance models: A review of seventy models, Renewable and Sustainable Energy Reviews 107 (2019) 374–387.

[19] G. Tina, P. S. bo, Case study of a grid connected with a battery photovoltaic system: V-trough concentration vs. single-axis tracking, Energy Conversion and Management 64 (2012) 569–578.

[20] J. Thoma, Simulation by bond graphs: introduction to a graphical method, Berlin: Springer.

[21] T. Hulkoff, Usage of highly accelerated stress test (hast) in solar module ageing procedures, Master of Science Thesis, Chalmers University of Technology, Sueden (2009) 572–575.

[22] P.-O. Logerais, O. Riou, R. Doumane, M. Balistrou, J.-F. Durastanti, Étude par simulation de l'influence du vieillissement et des conditions climatiques sur la production électrique d'un module photovoltaïque, 16èmes Journées Internationales de Thermique (JITH) 153 (2013) 1–5.

[23] F. Pern, A. Czanderna, K. Emery, , R. Dhere, Weathering degradation of eva encapsulant and the effect of its yellowing on solar cell efficiency, in Photovoltaic Specialists Conference (1991) 557–561.

[24] J. Nayak, D. K. Mishra, P. Pattanaik, Numerical modelling and simulation of a 1-d silicon solar cell, Materials Today: Proceedings https://doi.org/10.1016/j.matpr.2020.10.233 (2020) 1–4.

[25] M. Islam, A. Thakur, Two stage modelling of solar photovoltaic cells based on sb2s3 absorber with three distinct bu er combinations, Solar Energy 202 (2020) 304–315.

[26] M. Rosa-Clot, P. Rosa-Clot, G. Tina, P. Scandura, Submerged photovoltaic solar panel: Sp2, Renewable Energy 35 (2010) 1862–1865.

[27] G. M. Tina, F. B. Scavo, L. Merlo, F. Bizzarri, Comparative analysis of monofacial and bifacial photovoltaic modules for oating power plants, Applied Energy (2021) 281 (2012) 116084.

[28] A. Gagliano, G. M. Tina, S. Aneli, S. Nizeti, Comparative assessments of the performances of pv/t and conventional solar plants, Journal of Cleaner Production 219 (2021) 304–315.

[29] G. M. Tina, S. Gagliano, Probabilistic modelling of hybrid solar/wind power system with solar tracking system, Renewable Energy 36 (2011) 1719–1727.

[30] A. Awasthi, A. Shukla, M. M. S.R, C. Dondariya, K. Shukla, D. Porwal, G.Richhariya, Review on sun tracking technology in solar pv system, Energy Reports 6 (2020) 392–405.
[31] R. Fuentes-Morales, A. Diaz-Ponce, M. I. P. Cruz, P. Rodrigo, L. Valentin-Coronado, F. Martell-Chavez, C. A. Pineda-Arellano, Control algorithms applied to active solar tracking systems: A review, Solar Energy 212 (2020) 203–219.
[32] M. Thirunavukkarasu, Y. Sawle, A comparative study of the optimal sizing and management of off-grid solar/wind/diesel and battery energy systems for remote areas, Frontiers in Energy Research 9 (2021) 752043.